High speed and high power polarization insensitive germanium photodetector with lumped structure

Guanyu Chen,[1] Yu Yu,[1,*] Xi Xiao,[2] and Xinliang Zhang[1]

[1]*Wuhan National Laboratory for Optoelectronics & School of Optoelectronic Science and Engineering, Huazhong University of Science and Technology, Wuhan 430074, China*
[2]*State Key Laboratory of Optical Communication Technologies and Networks, Wuhan Research Institute of Posts Telecommunications, Wuhan 430074, China*
[*]*yuyu@mail.hust.edu.cn*

Abstract: We propose and demonstrate a high speed and high power polarization insensitive germanium photodetector (Ge PD) with lumped structure based on related parallel Ge absorption regions. Two absorption regions are double sides illuminated to optimize the space charge density and the two dimensional (2D) grating coupler is adopted for both coupling and polarization independent operation. Being different from previous reported high power scheme with separate absorption areas, the proposed structure is specifically designed with doubled but related Ge absorption regions, forming the equivalent parallel resistor and thus the parasitic parameter can be engineered to ensure a simultaneous large bandwidth. The bandwidth is measured to be >35 GHz, while the maximum current density is measured to be 1.152 $mA/\mu m^3$. The dark current and the responsivity of the proposed Ge PD are measured to be 1.82 μA and 1.06 A/W. Modulated signals experimentally validate the high speed operation and doubled power handling capacity for the proposed scheme. Furthermore, the bit error rate results show the superior performance for the proposed Ge PD at high photocurrent.

©2016 Optical Society of America

OCIS codes: (040.5160) Photodetectors; (060.5625) Radio frequency photonics; (130.0130) Integrated optics; (250.0250) Optoelectronics.

References and links

1. A. Seeds, "Microwave photonics," IEEE Trans. Microw. Theory Tech. **50**(3), 877–887 (2002).
2. V. J. Urick, F. Bucholtz, J. D. McKinney, P. S. Devgan, A. L. Campillo, J. L. Dexter, and K. J. Williams, "Longhaul analog photonics," J. Lightwave Technol. **29**(8), 1182–1205 (2011).
3. D. Marpaung, C. Roeloffzen, R. Heideman, A. Leinse, S. Sales, and J. Capmany, "Integrated microwave photonics," Laser Photonics Rev. **7**(4), 506–538 (2013).
4. T. Ishibashi and N. Shimizu, "Uni-traveling-carrier photodiodes," in Ultrafast Electron. Optoelectron. '97 Conf.,Incline Village, NV (1997).
5. M. Piels and J. E. Bowers, "40 GHz Si/Ge uni-traveling carrier waveguide photodiode," J. Lightwave Technol. **32**(20), 3502–3508 (2014).
6. X. Wang, N. Duan, H. Chen, and J. Campbell, "InGaAs–InP photodiodes with high responsivity and high saturation power," IEEE Photon. Technol. Lett. **19**(16), 1272–1274 (2007).
7. E. Rouvalis, F. N. Baynes, X. Xie, K. Li, Q. Zhou, F. Quinlan, T. M. Fortier, S. A. Diddams, A. G. Steffan, A. Beling, and J. C. Campbell, "High-power and high-linearity photodetector modules for microwave photonic applications," J. Lightwave Technol. **32**(20), 3810–3816 (2014).
8. X. Xie, Q. Zhou, E. Norberg, M. Jacob-Mitos, Y. Chen, A. Ramaswamy, G. Fish, J. E. Bowers, J. Campbell, and A. Beling, "Heterogeneously integrated waveguide-coupled photodiodes on SOI with 12 dBm output power at 40 GHz," in Optical Fiber Communication Conference, OSA Technical Digest (online) (OSA, 2015), paper Th5B.7.
9. A. Beling, H. Chen, H. Pan, and J. C. Campbell, "High-power monolithically integrated traveling wave photodiode array," IEEE Photonics Technol. Lett. **21**(24), 1813–1815 (2009).
10. N.-N. Feng, P. Dong, D. Zheng, S. Liao, H. Liang, R. Shafiiha, D. Feng, G. Li, J. E. Cunningham, A. V. Krishnamoorthy, and M. Asghari, "Vertical p-i-n germanium photodetector with high external responsivity integrated with large core Si waveguides," Opt. Express **18**(1), 96–101 (2010).

#260359 Received 2 Mar 2016; revised 15 Apr 2016; accepted 26 Apr 2016; published 28 Apr 2016

11. J. Michel, J. F. Liu, and L. C. Kimerling, “High-performance Ge-on-Si photodetectors,” Nat. Photonics **4**(8), 527–534 (2010).
12. C. T. DeRose, D. C. Trotter, W. A. Zortman, A. L. Starbuck, M. Fisher, M. R. Watts, and P. S. Davids, “Ultra compact 45 GHz CMOS compatible Germanium waveguide photodiode with low dark current,” Opt. Express **19**(25), 24897–24904 (2011).
13. S. Liao, N.-N. Feng, D. Feng, P. Dong, R. Shafiiha, C.-C. Kung, H. Liang, W. Qian, Y. Liu, J. Fong, J. E. Cunningham, Y. Luo, and M. Asghari, “36 GHz submicron silicon waveguide germanium photodetector,” Opt. Express **19**(11), 10967–10972 (2011).
14. G. Li, Y. Luo, X. Zheng, G. Masini, A. Mekis, S. Sahni, H. Thacker, J. Yao, I. Shubin, K. Raj, J. E. Cunningham, and A. V. Krishnamoorthy, “Improving CMOS-compatible Germanium photodetectors,” Opt. Express **20**(24), 26345–26350 (2012).
15. A. Novack, M. Gould, Y. Yang, Z. Xuan, M. Streshinsky, Y. Liu, G. Capellini, A. E. Lim, G. Q. Lo, T. Baehr-Jones, and M. Hochberg, “Germanium photodetector with 60 GHz bandwidth using inductive gain peaking,” Opt. Express **21**(23), 28387–28393 (2013).
16. L. Virot, L. Vivien, J.-M. Fédéli, Y. Bogumilowicz, J.-M. Hartmann, F. Bœuf, P. Crozat, D. Marris-Morini, and E. Cassan, “High-performance waveguide-integrated germanium PIN photodiodes for optical communication applications [Invited],” Photon.Res. **1**(3), 140–147 (2013).
17. G. Chen, Y. Yu, S. Deng, L. Liu, and X. Zhang, “Bandwidth improvement for germanium photodetector using wire bonding technology,” Opt. Express **23**(20), 25700–25706 (2015).
18. H. Chen, P. Verheyen, P. De Heyn, G. Lepage, J. De Coster, S. Balakrishnan, P. Absil, W. Yao, L. Shen, G. Roelkens, and J. Van Campenhout, “-1 V bias 67 GHz bandwidth Si-contacted germanium waveguide p-i-n photodetector for optical links at 56 Gbps and beyond,” Opt. Express **24**(5), 4622–4631 (2016).
19. K. J. Williams and R. D. Esman, “Design considerations for high-current photodetectors,” J. Lightwave Technol. **17**(8), 1443–1454 (1999).
20. M. Dentan and B. de Cremoux, “Numerical simulation of the nonlinear response of a p-i-n photodiode under high illumination,” J. Lightwave Technol. **8**(8), 1137–1144 (1990).
21. H. F. Taylor, O. Eknoyan, C. S. Park, K. N. Choi, and K. Chang, “Traveling wave photodetectors,” Proc. SPIE **1217**, 59–63 (1990).
22. A. Ramaswamy, M. Piels, N. Nunoya, T. Yin, and J. E. Bowers, “High power silicon-germanium photodiodes for microwave photonic applications,” IEEE Trans. Microw. Theory Tech. **58**(11), 3336–3343 (2010).
23. X. Luo, J. Song, X. Tu, Q. Fang, L. Jia, Y. Huang, T.-Y. Liow, M. Yu, and G.-Q. Lo, “Silicon-based traveling-wave photodetector array (Si-TWPDA) with parallel optical feeding,” Opt. Express **22**(17), 20020–20026 (2014).
24. C.-M. Chang, J. H. Sinsky, P. Dong, G. de Valicourt, and Y.-K. Chen, “High-power dual-fed traveling wave photodetector circuits in silicon photonics,” Opt. Express **23**(17), 22857–22866 (2015).
25. K. S. Giboney, M. J. W. Rodwell, and J. E. Bowers, “Travelling-Wave Photodetector Design and Measurements,” IEEE J. Sel. Top. Quantum Electron. **2**(3), 622–629 (1996).
26. M.-J. Lee, H.-S. Kang, and W.-Y. Choi, “Equivalent circuit model for Si avalanche photodetectors fabricated in standard CMOS process,” IEEE Electron Device Lett. **29**(10), 1115–1117 (2008).
27. K. J. Williams, R. D. Esman, and M. Dagenais, “Nonlinearities in p-i-n microwave photodetectors,” J. Lightwave Technol. **14**(1), 84–96 (1996).
28. M. Piels, A. Ramaswamy, and J. E. Bowers, “Nonlinear modeling of waveguide photodetectors,” Opt. Express **21**(13), 15634–15644 (2013).
29. J. Song, A. L. Eu-Jin, X. Luo, Y. Huang, X. Tu, L. Jia, Q. Fang, T. Y. Liow, M. Yu, and G. Q. Lo, “Microring resonator photodetector for enhancement in L-band performance,” Opt. Express **22**(22), 26976–26984 (2014).

1. Introduction

The photodetectors with large bandwidth, high saturation power and high linearity are greatly needed in optical communication, analog photonics and microwave photonics [1–3]. During the past decades, various kinds of high speed photodetectors with high-power handling capability based on III-V group materials have been demonstrated, such as the uni-traveling carrier (UTC) photodetector [4, 5], the modified UTC (MUTC) photodetector [6–8] and the traveling wave photodetector array [9]. However, it suffered from high cost, poor thermal conductivity and hard to realize large scale integration. By contrast, silicon based devices featured with low cost, high thermal conductivity and easy compatibility with complementary metal oxide semiconductor (CMOS) technology seems a possible solution for these problems. As one of the key components of silicon photonics, the waveguide coupling germanium photodetector (Ge PD) has attracted great attention during the last decade [10–18] and most of the researches focus on the improvement of the dark current [12], the responsivity [14] and the bandwidth [15,17]. It is very meaningful to improve both the bandwidth and saturation power of the Ge PD simultaneously.

The carrier transit time and RC parasitic parameter are the two main factors that limit the frequency response of the lumped Ge PD [17]. The high speed operation can be realized

#260359 Received 2 Mar 2016; revised 15 Apr 2016; accepted 26 Apr 2016; published 28 Apr 2016
(C) 2016 OSA

either by reducing the carrier transit time or the parasitic parameter. On the other hand, thermal failure [19] and space-charge effect [19,20] are the two main limiting factors for the saturation power. The thermal failure can be avoided by using high thermal conductivity material [7] while the space-charge effect can be reduced by optimizing the structure of the device or improving the carrier screening ability, such as making use of carrier velocity overshoot effects as in the UTC PD [1], adopting travelling wave configuration to reducing the space charge density [1,21] and increasing the applied voltage [19]. For silicon platform, the large thermal conductivity alleviates the thermal failure and improves the power handling capacity [22]. Although the Si/Ge UTC waveguide PD [22] and the parallel-fed travelling wave Ge PDs had been reported [23,24] to realize high power operation, the lower bandwidth in the UTC structure and the complicated design in the traveling structure restrict the applications.

In this paper, we therefore propose and demonstrate, a new kind of high speed and high power lumped Ge PD composed of two parallel and related Ge absorption regions. As the doubled Ge absorption regions share the same signal and ground electrodes, the equivalent parallel resistor is formed and the total junction resistance is halved. Therefore, the bandwidth of the proposed Ge PD is not degraded even if the total Ge area and junction capacitance are both doubled. Each Ge region is illuminated on both sides through the two dimensional (2D) grating coupler and thus the absorption region is more effectively used to realize an improved space charge density and thermal distribution. Besides, such a device is polarization independent due to the polarization diversity characterization of the 2D grating. Under 3V reverse biased voltage, the measured bandwidth for the proposed PD is >35 GHz at 0.42 mA photocurrent, while the measured maximum photocurrent is 28.8mA, which corresponds to a normalized photocurrent density of $1.152\ \text{mA}/\mu\text{m}^3$. The dark current and the responsivity for this new kind of Ge PD are $1.82\ \mu\text{A}$ and 1.06 A/W under 3V reverse biased voltage, while the values are $0.86\ \mu\text{A}$ and 1.01 A/W for the typical case under the same condition. The high speed experiments with modulated optical signal validate the high speed operation and doubled power handling capacity for the proposed Ge PD. Furthermore, the measured 10 Gb/s bit error rate (BER) results also validate the superior performance for the proposed Ge PD under high photocurrent.

2. Device design and fabrication

For comparison, three schemes are designed and fabricated. The structures of the typical one-side illuminated (type A), the double-side illuminated (type B) and the proposed (type C) Ge PDs are shown in Figs. 1(a) to 1(c).

For type A, the input light is illuminated from one side of the absorption region and a one dimensional (1D) grating is used for coupling. In this case, the input light will decay exponentially according to $\sigma(z)=\sigma(0)e^{-\Gamma\alpha z}$, where Γ is the confinement factor and α is the absorption coefficient of the Ge region [24, 25]. The simulated optical field absorption curve of the Ge-on-silicon (including the taper) structure is shown in Fig. 2(a), which shows that most of the light is absorbed in the input part of the Ge region. The end part of the Ge region is thus insufficiently used due to the weak optical field, as the simulated optical field distribution in Fig. 2(b) shown.

For type B, both sides of the Ge region are fully used by double sides illumination, as first proposed in [24], through a power splitter and a compact two-port 2D grating coupler. Compared with the single side illumination case in type A, where the increase of photocurrent is limited by the space charge effect and thermal failure within the characteristic length of the input part [24], the double sides illumination can improve the power handling capacity of the Ge PD as the input signal power on each input part is halved by the splitter, and thus the total power can be further increased before the space charge effect is taking effect. Besides, the double sides illumination will enlarge the maximum optical input power before thermal failure since the optical field distribution is more uniform, which can be observed clearly by

#260359 Received 2 Mar 2016; revised 15 Apr 2016; accepted 26 Apr 2016; published 28 Apr 2016
(C) 2016 OSA

comparing Fig. 2(b) to 2(e). However, such an improvement is limited for type B due to the limited and unchanged Ge region area [22–24].

Therefore, the doubled Ge regions are adopted for type C to further increase its power handling capacity. The four-port 2D grating is used for guiding the input light into both two sides of the Ge regions. The two Ge regions share the same signal (S) conductor of the lumped ground-signal-ground (GSG) electrode, which is also the typical lumped structure used in types A and B. Thus, the complexity of the electrode design and fabrication process for the proposed structure is not increased. It should be noted that the grating loss of the three different kinds of grating coupler have been taken out during the analysis for a more fair comparison.

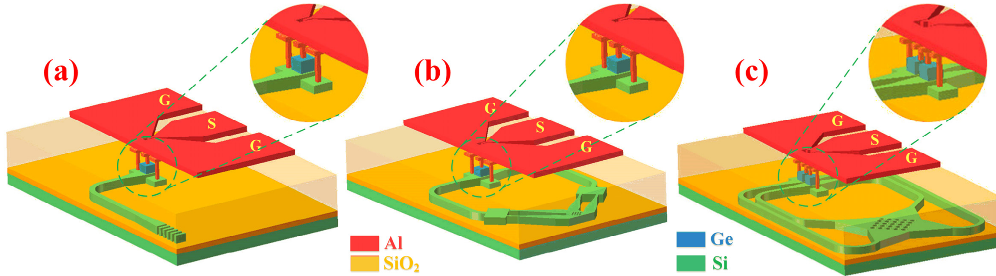

Fig. 1. Schematic layout of the Ge PD for (a) type A, (b) type B and (c) type C (dimensions are not drawn to scale).

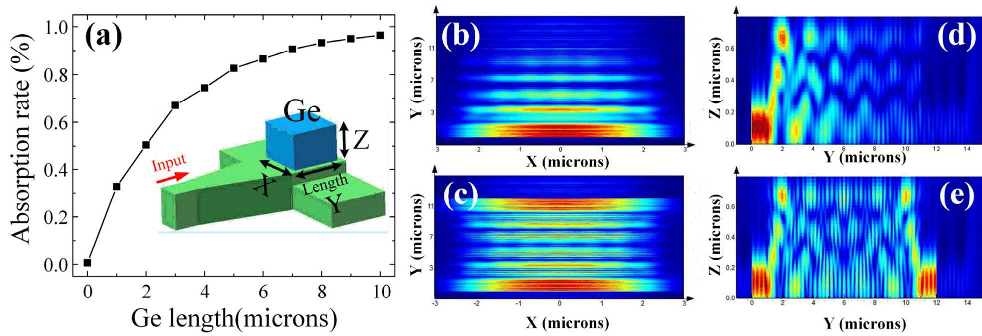

Fig. 2. (a) The simulated Ge absorption rate vs. Ge length for single side illuminated case (the inserted figure is the 3D schematic diagram of Ge region). The simulated optical field distribution at the XY cross section of the Ge region for Ge PDs with single-side (b) and double-sides illumination (c). The simulated optical field distribution at the YZ cross section of the Ge region for Ge PDs with single-side (d) and double-sides illumination (e).

Although the Ge absorption region is doubled to realized high power for type C, the large bandwidth can still be maintained based on the equivalent parallel junction resistor structure. In order to further understand its operation principle, the equivalent circuit model is adopted [15, 17, 18, 26]. For the typical Ge PIN PD (type A/B), it can be modeled as a simple RC circuit, as shown in Fig. 3(a). In this circuit, C_{pd} is the junction capacitance, R_{pd} is the series resistance, R_{load} is the equivalent load resistance and C_{load} is the equivalent load capacitance. The cut off frequency of this equivalent RC circuit is usually described as Eq. (1).

$$f_{RC}=\frac{1}{2\pi(R_{pd}+R_{load})(C_{pd}+C_{load})} \tag{1}$$

For the proposed design of type C, both N++ regions on the top of each Ge region connect the common signal electrode (positive pole) while the P++ regions in the silicon share the same

#260359 Received 2 Mar 2016; revised 15 Apr 2016; accepted 26 Apr 2016; published 28 Apr 2016
(C) 2016 OSA

ground electrode (negative pole). Therefore, the total equivalent junction resistance/capacitance of the new design can be equivalent to the result of two resistors/capacitors in parallel, as shown in Fig. 3(b). The total junction resistance will be halved while the total capacitance will be doubled theoretically according to the basic circuit theory. Therefore, the cut off frequency of the proposed Ge PD can be described as Eq. (2).

$$f_{RC}=\frac{1}{2\pi(R_{pd}/2+R_{load})(2C_{pd}+C_{load})} \tag{2}$$

Due to the narrow intrinsic region of the Ge PD, the carrier transit time is small enough and can be largely ignored [15, 17]. Therefore, according to the Eq. (1) to (2), the bandwidth for type A/B and type C can be calculated, as shown in Fig. 3(c). In Table 1, C_{pd} and R_{pd} are the experimentally extracted value, while C_{load} and R_{load} are obtained from the simulation results. Figure 3(c) shows that the large bandwidth for type C will be maintained because the increased capacitance is almost totally counteracted by the reduced resistance.

Table 1. Fit Parameters Used in the Simulation

Parameter	Type A/B	Type C
C_{pd}	10 fF	20 fF
R_{pd}	200 Ohm	100 Ohm
C_{load}	10 fF	10 fF
R_{load}	50 Ohm	50 Ohm

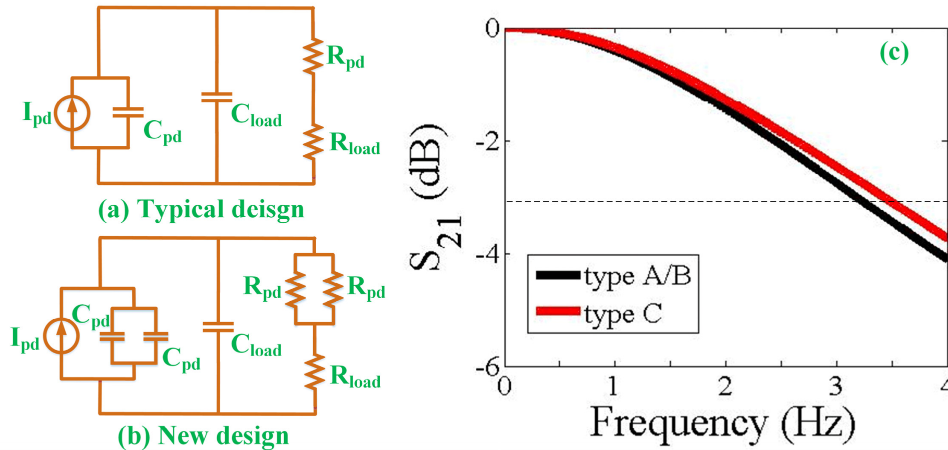

Fig. 3. Equivalent circuit model of the (a) typical and (b) the new Ge PD; the simulated S_{21} for type A/B and type C.

The devices are fabricated on the 220 nm thick silicon on insulator (SOI) wafer with 2 µm buried oxide (BOX) at the Institute of Microelectronics (IME) in Singapore. The input light propagates along the 0.5 µm wide single mode channel waveguide into the Ge absorption region and a 40 µm long taper is used for transition between the single mode waveguide and the multi-mode region below the Ge region. The etch depth for both the 1D and 2D grating is 70 nm. The width, length and height are 5 µm, 10 µm and 500 nm for single Ge region. The double-layer metals are deposited on it to form the electrode. Figure 4(a) is the cross section of the device and the microscopic images of the devices are shown in Figs. 4(b) to 4(d), corresponding to types A, B and C.

#260359 Received 2 Mar 2016; revised 15 Apr 2016; accepted 26 Apr 2016; published 28 Apr 2016
(C) 2016 OSA

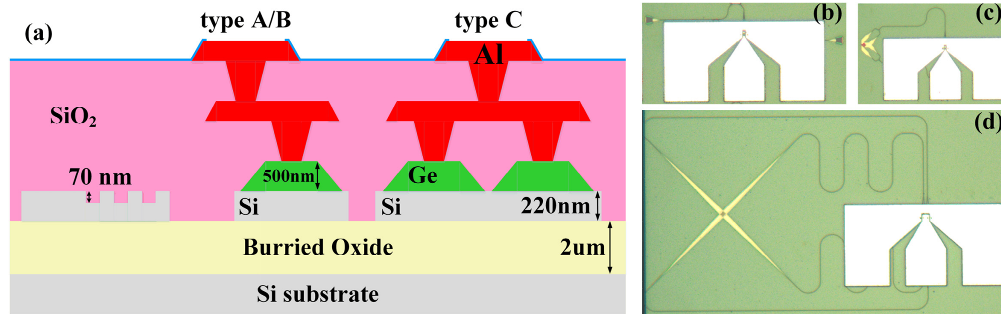

Fig. 4. (a) Cross section of the Ge PD; microscopic image of type A (b), type B (c) and type C (d).

3. Device characterization

The DC test is performed for the three kinds of Ge PDs. The dark current is first measured and the results are shown in Fig. 5(a). Similar results can be observed for types A and B while the dark current is doubled for type C, due to the doubled Ge absorption regions. Under 3 V reverse biased voltage, the dark currents are about 0.86, 0.89 and 1.82 μA for types A, B and C, respectively. Then the photocurrents under different input optical power are measured, as shown in Fig. 5(b). During the measurement, the optical amplifier and attenuator is used to change the input optical power. It can be seen from Fig. 5(b) that the measured maximum photocurrent is about 15.6, 18.8 and 28.8 mA for the three Ge PDs when the net optical power in the waveguide is 18 dBm and the reverse biased voltage is 3 V. To be noted the measured optical power for type C has not reached the saturation value due to the power limitation of the available optical amplifier for signal inputting. However, it still can be seen from Fig. 5(b) that the proposed structure presents superior performance in terms of the high saturation power and the large linear region. In the linearity region, the responsivities are calculated to be 1.01, 0.99 and 1.06 A/W under 3 V reverse biased voltage for types A, B and C, respectively.

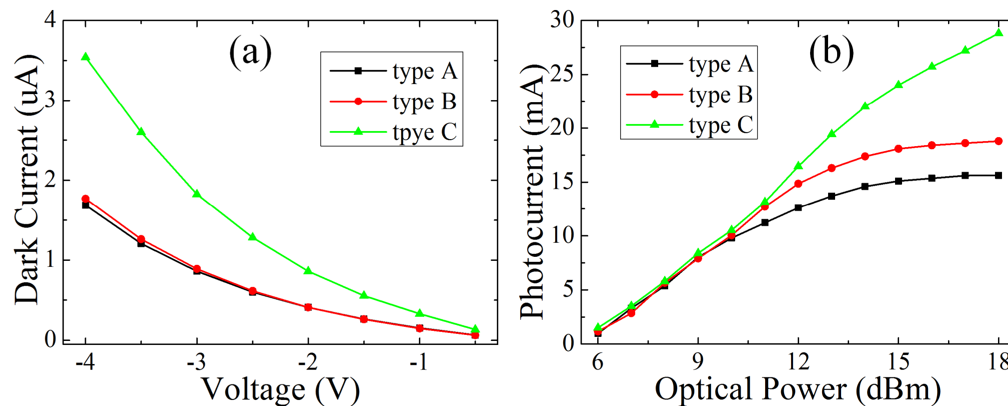

Fig. 5. (a) Dark current for three kinds of Ge PDs; (b) photocurrent as a function of input optical for three kinds of Ge PD under 3 V reverse biased voltage.

Then the bandwidth is measured under 3V reverse biased voltage and 0.42 mA photocurrent, and the S_{21} results are shown in Fig. 6(a). The bandwidths are 35.4, 35.91 and 35.84 GHz for types A, B and C. It will decrease under high photocurrent condition because of the nonlinearity characteristic and space charge effect [24,27,28]. Figure 6(b) shows the measured S_{21} for the three kinds of PDs, at different photocurrents. Under a photocurrent of 13 mA, the bandwidth degrades to 0.75, 0.89 and 9.13 GHz for types A, B and C,

#260359 Received 2 Mar 2016; revised 15 Apr 2016; accepted 26 Apr 2016; published 28 Apr 2016
(C) 2016 OSA

respectively. The normalized RF output of type C is larger than type A and B at high photocurrent, which validates its superior power handling capacity.

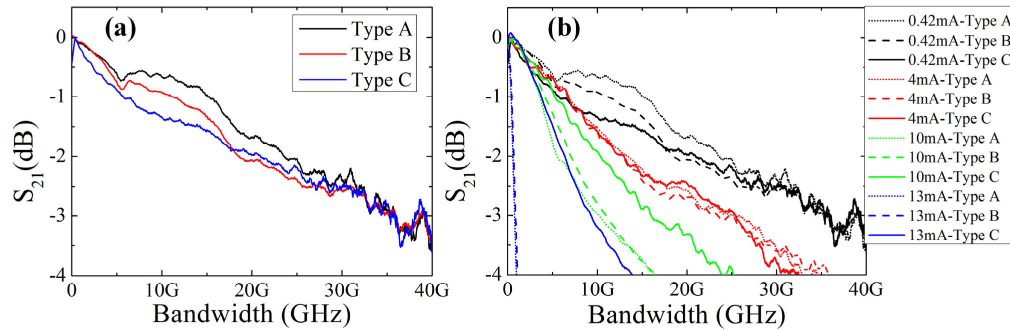

Fig. 6. (a) The measured S_{21} for the three kinds of Ge PD when the reverse biased voltage is 3V and the photocurrent is 0.42 mA. (b) The measured S_{21} for the three kinds of Ge PD when the reverse biased voltage is 3V and the photocurrent is on different level.

To verify the previous equivalent circuit model analysis, the series resistance of the Ge PD is extracted by measuring the forward biased photocurrent from + 0.5 to + 1V, which is a commonly used method [10, 13, 14, 16]. The total resistance for the typical (type A) and the proposed (type C) Ge PDs are measured to be 230 and 149 Ω, respectively. Considering the 50 Ω cable impedance, the total junction resistance for types A and C can be roughly estimated as 180 and 99 Ω, respectively. It can be concluded that the total junction resistance is reduced due to the parallel structure. Besides, the total capacitance can also be estimated as 19.55 and 29.8 fF for types A and C based on Eq. (1) and (2). It should be noted that the estimated capacitance contains not only the junction capacitance but also the parasitic load capacitance between the pads. According to our simulation results, the parasitic load capacitance between the pads is about 10 fF. The junction capacitance is thus estimated as 9.55 and 19.8 fF for types A and C, which validate the junction capacitance of the proposed high power Ge PD is doubled due the parallel capacitor structure. The extracted relative large R_{pd} compared with some literatures [10, 16] might be due to the different Ge region structure or different doping density. The small difference between the measured values and the fit parameters in Table 1 may be due to either fabrication variation of the PIN junction or an inexact fit of the Ge photodetector response. However, it still can be concluded that the total bandwidth of the type C Ge PD will be maintained because the doubled capacitance is counteracted by the halved capacitance.

In order to fully characterize the high speed and high power performance, the modulated signal at 10 Gb/s bit rates are utilized, with pseudo random bit sequence (PRBS) of 2^{15}-1. The signals are coupled into the Ge PDs through the 1D/2D grating couplers. The converted RF signal is then injected into the digital communication analyzer (DCA: Agilent 86100C) for characterization while the reverse bias from the source meter (Keysight B2902A) is loaded on the chip through a bias-tee. The measured eye diagrams for the three types PDs are shown in Fig. 7. All the Ge PDs show clear and open eye diagrams at lower photocurrent. The eye diagram begins to degrade when the photocurrent beyond 8 mA for type A and 11 mA for type B. By contrast, the threshold photocurrent of type C can be up to 16 mA. The measured RF power is about 2.6, 3.6 and 6 dBm for types A, B and C when the photocurrent is 18 mA. The improved power handling capacity accords well with the DC results in Fig. 5(b).

#260359 Received 2 Mar 2016; revised 15 Apr 2016; accepted 26 Apr 2016; published 28 Apr 2016
(C) 2016 OSA

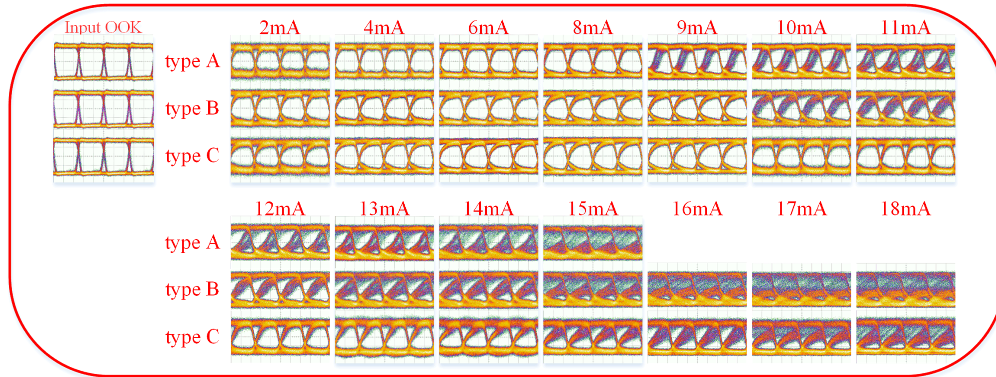

Fig. 7. The measured 10 Gb/s eye diagrams for the three kinds of Ge PDs under different photocurrent.

To quantitatively verify the power handling capacity, the 10 Gb/s BER measurements are further performed for demonstration. The BERs are measured for four different regions, considering the linear and saturated regions for different types, namely 2, 8, 11 and 13 mA in Fig. 5(b). For each fixed photocurrent, different BER values from the error analyzer (EA) under different RF powers are recorded by controlling a tunable RF attenuator. The results are plotted in Figs. 8(a) to 8(d). It can be concluded that the similar BER results can be observed when the three kinds of Ge PDs are operated in the linear region. With the increase of the photocurrent, the difference becomes obvious, and the superiority for type C Ge PD is getting larger. The BER is hard to measure when the photocurrent beyond 11 mA for type A and 13 mA for type B.

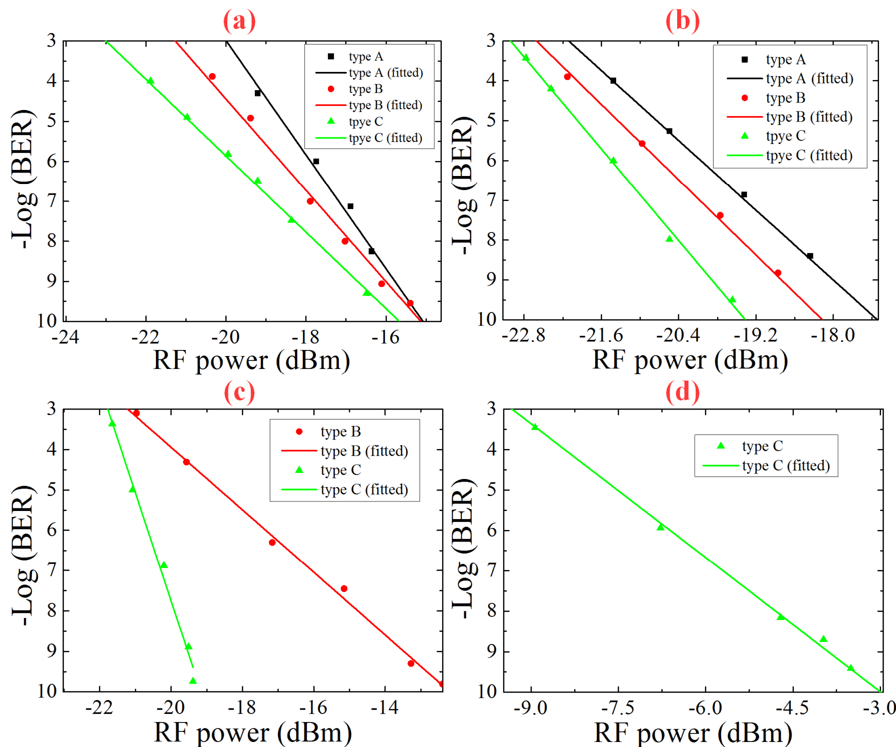

Fig. 8. The measured 10 Gb/s BER as a function of different RF power for the three kinds of Ge PDs when the photocurrent is (a) 2 mA, (b) 8 mA, (c) 11 mA, (d) 13 mA.

#260359 Received 2 Mar 2016; revised 15 Apr 2016; accepted 26 Apr 2016; published 28 Apr 2016
(C) 2016 OSA

It is worth noting that since the 2D grating coupler is utilized in the proposed structure, the Ge PD is polarization insensitive and can be very useful for the applications of polarization transparent or polarization multiplexed systems. Other 1 to 4 power splitters can also be utilized to achieve the same functionality.

4. Discussion

High power Ge PD have been demonstrated either based on the large evanescently coupled Ge PD [22] or traveling wave array structure [23, 24]. The comparison between the high power Ge PD in literatures and our proposed structure is shown in Table 2. For large evanescently coupled Ge PD, the small bandwidth and the large dark current usually will be the limiting factors due the large cross section of the Ge absorption. On the other hand, for the traveling wave array structure, the complicated design of the electrode restricts its practicability and the bandwidth will also be limited by the parasitic parameters [23]. Besides, the dark current usually will be affected by the multiple stages of Ge absorption regions and the traveling wave electrode [24]. Based on the double sides illumination structure, the Ge absorption region is more effectively used and the photocurrent desity is thus improved greatly, as can be seen from Table 2. The power handling capacity is further doubled based on the two related Ge aborption regions while the large bandwidth is maintained at the same time because the equivalent resistance is halved. Moreover, the device features with low dark current and high responsivity.

It should be noted that the doubled and related Ge regions are different from single Ge region with doubled length, in terms of power handling capacity. The improvement of power handling capacity is limited by simply doubling the PD length, because the input light is exponential absorbed in the Ge region and the increased length will not fully contribute to the photocurrent, in the case of large input optical power. However, in the proposed scheme, the Ge region is more effectively used by dividing and feeding the input power into several parts with separate but related configuration. The distribution of space charge will be more uniform, and the power handling capacity is thus improved significantly.

The bandwidth of the lumped Ge PD can be further improved though the gain peaking technology, which can be realized either based on the on chip [15] or the off chip inductor [17]. The saturation power of the lumped Ge PD can also be further enhanced by increasing the number of the related parallel Ge absorption regions. However, the large bandwidth will degrade even the equivalent junction resistance is reduced for the multiple parallel Ge absorptions. For example, if nine related Ge absorption region forming the parallel structure, the equivalent junction resistance will reduce to one ninth of the single Ge case while the equivalent junction capacitance will increase nine fold. Based on the fit parameter in Table 1 and the equivalent model in Fig. 2, the bandwidth can be roughly estimated as 22 GHz. Therefore, the further increasement of the saturation power is at the expense of the degradation of its bandwidth.

On the other hand, the increase of the related Ge absorption regions is also restricted by the lumped model. Usually, the related Ge regions should have a certain distance because the slope profile of the grown Ge region [29]. Taking both the Ge width and distance between each Ge regions into consideration, the device will be too big to treat as a lumped model if more Ge regions are introduced [21, 23, 24]. Therefore, the related parallel two Ge absorption regions is preferable for realizing both large bandwidth and high power. It should be noted that the idea of double sides illumination and equivalent parallel resistance is universal for improving both the bandwidth and the power handling capacity at the same time. For instance, the double sides and parallel resistance structure can be combined with the large cross section Ge absorption region and multiple stages traveling structure to improve both its bandwidth and power handling capacity.

5. Conclusion

We propose and demonstrate a new kind of high speed and high power polarization insensitive lumped Ge PD based on two parallel and related Ge absorption regions. Thanks to

#260359 Received 2 Mar 2016; revised 15 Apr 2016; accepted 26 Apr 2016; published 28 Apr 2016
(C) 2016 OSA

the equivalent parallel resistor formed by the doubled parallel Ge regions, the high speed is realized while the power handling capacity is also doubled. The measured bandwidth under 3V reverse biased voltage and 0.42 mA photocurrent is 35.84 GHz for the proposed Ge PD while the measured maximum photocurrent is 28.8 mA. The high speed operation and doubled power handling capacity for the proposed Ge PD are achieved. Besides, the BER measurement is performed and the results shown the superior performance of the proposed Ge PD under high photocurrent.

Table 2. Comparison of the High Power Ge PD in Literature and our Work

Year	Dark current	Responsivity	Maximum current	Maximum current density	Bandwidth	Ref.
2010	125 μA @-8V	0.8 A/W @-7V	125.49 mA @-8V	0.04 $mA/\mu m^3$	4.38 GHz @-5V	[22]
2014	/	0.82 A/W @-4V	65 mA @-4V	>0.32 $mA/\mu m^3$	20 GHz @-4V	[23]
2015	59.2 μA @-3V	0.76A/W @-3V	112 mA @-3V	/	32.5 GHz @-3V & 0.3 mA	[24]
2016	1.82 μA @-3V	1.06 A/W @-3V	28.8 mA @-3V	1.152 $mA/\mu m^3$	35.84 GHz @-3V & 0.42 mA	This work

Acknowledgments

This work was supported by the National Natural Science Foundation of China (NSFC) (Grant No. 61475050 and 61275072), the New Century Excellent Talent Project in Ministry of Education of China (NCET-13-0240), the Fundamental Research Funds for the Central Universities (HUST2015TS079), and Huawei Technologies Co. Ltd..